Bulk simulation of polar liquids in spherical symmetry.

Stenhammar, Joakim; Linse, Per; Karlström, Gunnar

Published in:
Journal of Chemical Physics

DOI:
10.1063/1.3352423

2010

Bulk simulation of polar liquids in spherical symmetry

Joakim Stenhammar,[1,a)] Per Linse,[1] and Gunnar Karlström[2]
[1]*Division of Physical Chemistry, Center for Chemistry and Chemical Engineering, Lund University, P.O. Box 124, S-221 00 Lund, Sweden*
[2]*Division of Theoretical Chemistry, Center for Chemistry and Chemical Engineering, Lund University, P.O. Box 124, S-221 00 Lund, Sweden*

(Received 14 December 2009; accepted 11 February 2010; published online 10 March 2010)

Molecular simulations of strongly coupled dipolar systems of varying size have been carried out, using particles confined inside a dielectric cavity and an image charge approach to treat the dielectric response from the surroundings. A simple method using penalty functions was employed to create an isotropic and homogeneous distribution of particles inside the cavity. The dielectric response of the molecular system was found to increase as the number of particles N was increased. Nevertheless, a significant surface effect remained even for the largest systems ($N=10\,000$), manifesting itself through a decrease in the dielectric constant of the system as the confining surface was approached. The surface effect was significantly reduced by using a negative dielectric constant of the surrounding dielectric medium, although accomplishing a full dielectric solvation of the molecular system was not possible. © *2010 American Institute of Physics*. [doi:10.1063/1.3352423]

I. INTRODUCTION

The simulation of Coulombic and dipolar bulk systems poses a great problem due to the long-range nature of the intermolecular interactions present in these systems. Several ways have been proposed to overcome these obstacles, the two most popular ones being the lattice summation technique due to Ewald[1] and the reaction field (RF) technique due to Barker and Watts.[2] In a recent paper,[3] however, we showed that both these techniques suffer from artifacts created by the cubic symmetry, leading to an anisotropy of the simulated system, which is unwanted in bulk simulations. Such effects have been pointed out before for both biomolecular[4,5] and ionic[6] systems simulated using the Ewald summation technique, and attempts have also been made to overcome these periodicity artifacts.[7,8] A method that avoids the cubic symmetry of the Ewald and RF methods was developed by Friedman[9] in 1975, whose ideas built on the so-called method of images[10] to represent the reaction field from a dielectric medium outside a spherical cavity enclosing the molecular system. Although Friedman's method has been tested in practice a few times,[11,12] it has not rendered much interest in the simulation of Coulombic or dipolar systems, largely due to the inherent inhomogeneity and anisotropy of the systems. In particular, the study by Wang and Hermans[12] on water points out that (i) the surface effects become large when the coupling between the molecular system and the surrounding dielectric medium is large and (ii) to reduce the surface effects, one has to limit the strength of the coupling to the surroundings, leading to a smaller solvation of the molecular system than desired.

In the present contribution, we will review the use of image charges and dipoles as developed by Friedman for the simulation of a simple dipolar system and assess a simple scheme to reduce the surface effects. Furthermore, we will analyze the dielectric behavior of the simulated systems using dielectric fluctuation formulas developed recently.[13]

II. THEORY

A. Electric fluctuations in dielectric media

In a previous paper,[13] we derived expressions describing the electric multipole moment fluctuations in a dielectric medium. One of the main results was that the probability distribution $P(Q_{\ell 0})$ of the axial component of a spherical 2^ℓ-pole moment $Q_{\ell 0}$ (M_ℓ in our previous notation) of a spherical subvolume inside a dielectric medium of infinite extension is described by the Gaussian function

$$P(Q_{\ell 0}) = \tilde{a} e^{-\tilde{\alpha} Q_{\ell 0}^2}, \tag{1}$$

with the exponent $\tilde{\alpha}$ given by

$$\tilde{\alpha} = \frac{(2\ell+1)^2 \varepsilon}{2(\varepsilon-1)\ell[(\ell+1)\varepsilon+\ell]} \frac{1}{R_{\text{diel}}^{2\ell+1} kT}, \tag{2}$$

where R_{diel} represents the radius of the sphere, ε the dielectric constant of the medium, k Boltzmann's constant, T the absolute temperature, and $Q_{\ell m}$ the spherical electric multipole moment defined by

$$Q_{\ell m} \equiv \int_V d\mathbf{r} \rho(\mathbf{r}) r^\ell C_{\ell m}(\Omega). \tag{3}$$

In Eq. (3), $\rho(\mathbf{r})$ is the volume charge density at $\mathbf{r}$ and $C_{\ell m}(\Omega)$ represents Racah's unnormalized spherical harmonics. The Gaussian form of Eq. (1) means that the mean-square multipole moment $\langle Q_{\ell 0}^2 \rangle$ can be expressed as

$$\langle Q_{\ell 0}^2 \rangle = (2\tilde{\alpha})^{-1}. \tag{4}$$

In the case when the dielectric constant $\varepsilon_{\text{diel}}$ of the sphere and ε_{sur} of the surrounding medium are different and the

a)Electronic mail: joakim.stenhammar@fkem1.lu.se.

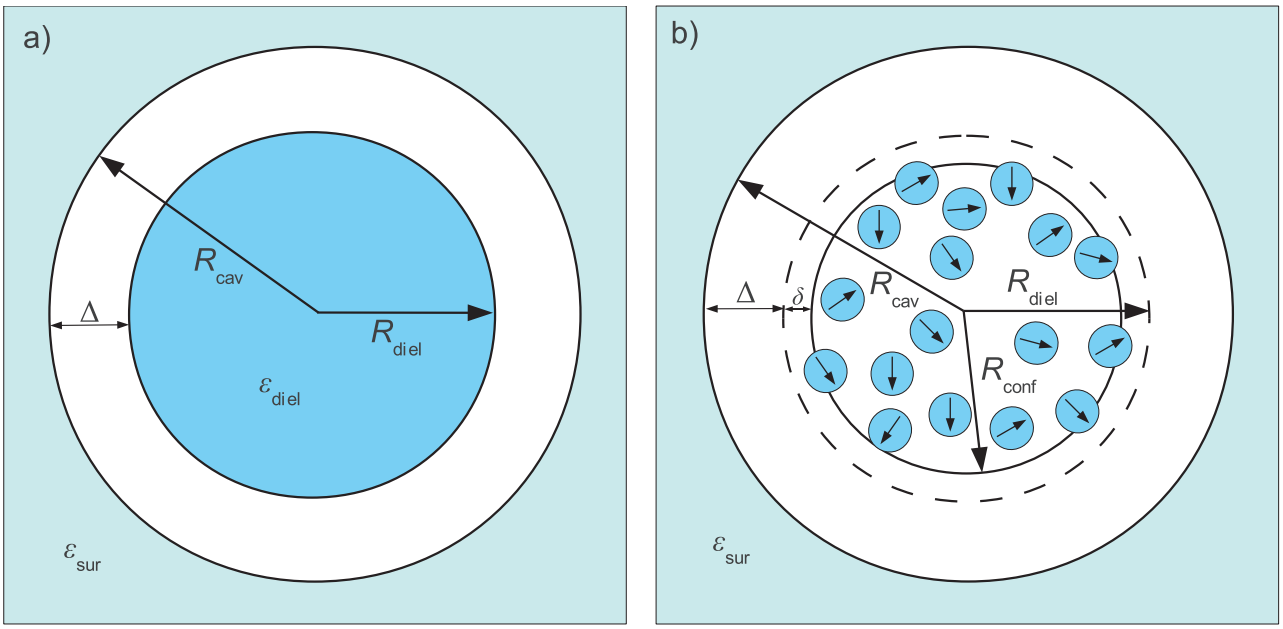

FIG. 1. Schematic description of (a) the dielectric model and (b) the simulated systems. The dashed circle in the right panel indicates that R_{diel} appears as a fitting parameter in the simulated systems.

reaction potential of the surrounding dielectric is applied at a distance Δ outside the dielectric sphere [see Fig. 1(a)], a small generalization of the derivation in Ref. 13 leads to the following expression for $\langle Q_{\ell 0}^2(\Delta)\rangle$:

$$\langle Q_{\ell 0}^2(\Delta)\rangle = \left[\frac{\ell(\varepsilon_{diel}+1)+1}{\ell(\varepsilon_{diel}-1)R_{diel}^{2\ell+1}kT} - \frac{(\ell+1)(\varepsilon_{sur}-1)}{[(\ell+1)\varepsilon_{sur}+\ell](R_{diel}+\Delta)^{2\ell+1}kT} \right]^{-1}. \quad (5)$$

By putting $\varepsilon_{diel}=\varepsilon_{sur}=\varepsilon$ together with $\Delta=0$ in Eq. (5) and the subsequent use of Eq. (4), one recovers Eq. (2).

To facilitate the comparison between multipole moments of different order ℓ, it is convenient to introduce the scaled quantity $\hat{Q}_\ell(\Delta)$ defined by

$$\hat{Q}_\ell(\Delta) \equiv \langle Q_{\ell 0}^2(\Delta)\rangle R_{diel}^{-(2\ell+1)}, \quad (6)$$

where we have dropped the subscript m, since we will henceforth only be interested in the axial components of the electric multipole moments. It is clear from Eqs. (5) and (6) that $\hat{Q}_\ell(\Delta)$ depends on the ratio Δ/R_{diel}, rather than on R_{diel} and Δ separately. The exclusion of the nonaxial components of the multipole moments $Q_{\ell m}$, $m\neq 0$, from the analysis is motivated by the spherical symmetry of the investigated systems, leading to that all directions become equivalent.

B. The method of images

The so-called *method of images* is a standard strategy for solving Poisson's equation subject to certain boundary conditions.[10] The method gets its name from the fact that the reaction potential of the induced surface charge density created by a source charge q near a dielectric discontinuity may be represented by the potential from one or several *image charges*, whose magnitudes and positions depend on the distance between q and the dielectric discontinuity, the dielectric constants of the dielectric media, and the shape of the discontinuity.

In 1975, Friedman[9] derived an expression for the reaction potential ϕ_r originating from a charged particle inside a spherical cavity of radius R_{cav} with $\varepsilon=1$ surrounded by a dielectric medium with the dielectric constant ε_{sur}. It turns out that ϕ_r can be written as a series expansion according to

$$\phi_r = \phi^{(0)} + \phi^{(1)} + \phi^{(2)} + \cdots \quad (7)$$

where

$$\phi^{(k)} \propto \frac{\varepsilon_{sur}-1}{(\varepsilon_{sur}+1)^{k+1}}. \quad (8)$$

In this case, the image charge approximation proposed by Friedman consists in putting $\phi_r=\phi^{(0)}$ and ϕ_r can then be viewed as arising from a single image charge. Furthermore, the higher terms in the expansion become zero in the limit $\varepsilon_{sur}\to\infty$. For a high dielectric medium with a dielectric constant similar to that of water, the error in ϕ_r introduced by the zeroth-order truncation of Eq. (7) is less than 1%.[9]

Furthermore, the method can easily be extended to ideal dipoles inside the cavity.[9] In this case, the zeroth-order reaction potential $\phi^{(0)}$ originating from a dipole μ_i at position $\mathbf{r}_i$ can be written as the sum of the potential of an image charge q_i^* and an image dipole $\boldsymbol{\mu}_i^*$, both located at $\mathbf{r}_i^*$, according to

$$\mathbf{r}_i^* = \mathbf{r}_i(R_{cav}/r_i)^2, \quad (9a)$$

$$q_i^* = \frac{\varepsilon_{sur}-1}{\varepsilon_{sur}+1}\frac{R_{cav}\cos\theta}{r_i^2}\mu_i, \quad (9b)$$

$$\mu_{i,\|}^* = \frac{\varepsilon_{sur}-1}{\varepsilon_{sur}+1}\left(\frac{R_{cav}}{r_i}\right)^3\mu_{i,\|}, \quad (9c)$$

$$\mu_{i,\perp}^{*} = -\frac{\varepsilon_{\mathrm{sur}}-1}{\varepsilon_{\mathrm{sur}}+1}\left(\frac{R_{\mathrm{cav}}}{r_i}\right)^3 \mu_{i,\perp}, \tag{9d}$$

where θ is the angle between $\boldsymbol{\mu}_i$ and $\mathbf{r}_i$, and $\mu_{i,\parallel}$ and $\mu_{i,\perp}$ the components of $\boldsymbol{\mu}_i$ parallel and perpendicular to $\mathbf{r}_i$, respectively. Due to the high accuracy of the image charge approximation for high dielectric media, the method seems suitable for the simulation of waterlike systems. Henceforth, we will refer to Friedman's simulation technique as *image boundary conditions* (IBCs).

Equation (9a) shows that for configurations where $r_i = R_{\mathrm{cav}}$, we get $\mathbf{r}_i^{*} = \mathbf{r}_i$, leading to a divergence in the interaction energy. Hence, care needs to be taken so as to avoid such configurations. One possible strategy is to confine the particles within a sphere of radius $R_{\mathrm{conf}} < R_{\mathrm{cav}}$ [see Fig. 1(b)], thus enforcing that $r_i < r_i^{*}$. Although this strategy helps avoiding the divergence at $r_i = R_{\mathrm{cav}}$, configurations where the source particle is close to the dielectric discontinuity, and thus to its image particle, will still be energetically favored. This will inevitably enhance the inhomogeneous density and nonisotropic orientation of the particles near the cavity surface; an effect which is unwanted if one wishes to simulate a bulk liquid. To remedy this problem, we will use an energetic penalty function u_{pen} given by

$$u_{\mathrm{pen}}(r,\theta) = u_r(r) + u_\theta(r)\cos^2\theta, \tag{10}$$

to create a uniform density and orientation distribution of the particles. Further details about the radial and orientational penalty functions $u_r(r)$ and $u_\theta(r)\cos^2\theta$ are given in Sec. III B.

III. MODEL AND METHODS

A. Molecular model

The molecular model system is composed of N particles confined inside a spherical volume of radius R_{conf} at a temperature T. The potential energy U of the system is assumed to be pairwise additive according to

$$U = \sum_{i=1}^{N-1}\sum_{j=i+1}^{N} u_{ij}(r_{ij}) + \sum_{i=1}^{N}\sum_{j=1}^{N} u_{ij}^{*}(r_{ij}). \tag{11}$$

The direct interaction u_{ij} between particles i and j is composed of a Lennard-Jones (LJ) and a dipole-dipole potential (also referred to as a Stockmayer potential) according to

$$u_{ij}(r_{ij}) = u_{ij}^{\mathrm{LJ}}(r_{ij}) + u_{ij}^{\mathrm{dd}}(r_{ij}), \tag{12}$$

with

$$u_{ij}^{\mathrm{LJ}}(r_{ij}) = 4\epsilon\left[\left(\frac{\sigma}{r_{ij}}\right)^{12} - \left(\frac{\sigma}{r_{ij}}\right)^{6}\right], \tag{13}$$

$$u_{ij}^{\mathrm{dd}}(r_{ij}) = \frac{1}{4\pi\varepsilon_0}\left[\frac{\boldsymbol{\mu}_i\cdot\boldsymbol{\mu}_j}{r_{ij}^3} - \frac{3(\boldsymbol{\mu}_i\cdot\mathbf{r}_{ij})(\boldsymbol{\mu}_j\cdot\mathbf{r}_{ij})}{r_{ij}^5}\right], \tag{14}$$

where the size parameter σ and interaction parameter ϵ characterize the LJ interaction, $\boldsymbol{\mu}_i$ denotes the dipole vector of particle i, $\mathbf{r}_{ij}$ is the vector between particle i and j, and $r_{ij} = |\mathbf{r}_{ij}|$. Furthermore, the image interaction energy u_{ij}^{*} between particle i and the image of particle j is given by

$$u_{ij}^{*}(r_{ij}) = -\frac{1}{2}\frac{1}{4\pi\varepsilon_0}\left[\frac{\boldsymbol{\mu}_i\cdot\mathbf{r}_j^{*}}{(r_{ij}^{*})^3}q_j^{*} - \frac{\boldsymbol{\mu}_i\cdot\boldsymbol{\mu}_j^{*}}{(r_{ij}^{*})^3} + \frac{3(\boldsymbol{\mu}_i\cdot\mathbf{r}_{ij}^{*})(\boldsymbol{\mu}_j^{*}\cdot\mathbf{r}_{ij}^{*})}{(r_{ij}^{*})^5}\right], \tag{15}$$

where $\mathbf{r}_j^{*}$, q_j^{*}, and $\boldsymbol{\mu}_j^{*}$ are given by Eq. (9), $\mathbf{r}_{ij}^{*}$ denotes the vector between particle i and the image of particle j, and $r_{ij}^{*} = |\mathbf{r}_{ij}^{*}|$. The factor 1/2 in Eq. (15) comes from the fact that u_{ij}^{*} represents a polarization interaction. Furthermore, the total electrostatic energy U_{el} of the system is given by

$$U_{\mathrm{el}} = \sum_{i=1}^{N-1}\sum_{j=i+1}^{N} u_{ij}^{\mathrm{dd}}(r_{ij}) + \sum_{i=1}^{N}\sum_{j=1}^{N} u_{ij}^{*}(r_{ij}). \tag{16}$$

Throughout, we have used the LJ parameters $\sigma = 2.8863$ Å and $\epsilon = 1.97\,023$ kJ mol^{-1} and the dipole moment $\mu = 0.34\,397e$ Å (corresponding to 0.65 atomic units) at temperature $T = 315.8$ K, which is identical to the parameters used in Ref. 3. In reduced units, the system is characterized by the quantities $\mu^{*} \equiv \mu/(4\pi\varepsilon_0\epsilon\sigma^3)^{1/2} = 1.863$ and $T^{*} \equiv kT/\epsilon = 1.333$.

For comparison, some results obtained from the same system but simulated using the Ewald summation technique are included in the study. Detailed specifications of these simulations were given in Ref. 3. When nothing else is explicitly stated, the number density of the Ewald system is ≈3% higher than that of the IBC systems.

B. Penalty function

To accomplish a uniform particle density and orientation distribution within the confining sphere, a penalty function u_{pen} was applied to each particle in the system in accordance with Eq. (10). The functions $u_r(r)$ and $u_\theta(r)$ entering in Eq. (10) were updated at regular intervals according to

$$u_r^{(k)}(r) = u_r^{(k-1)}(r) + skT\ln(\rho(r)/\bar{\rho}), \tag{17}$$

$$u_\theta^{(k)}(r) = u_\theta^{(k-1)}(r) + skT\ln[(\rho(r)/\bar{\rho})3\langle\cos^2\theta\rangle_r], \tag{18}$$

where superscript k denotes the order of the iteration, $\rho(r)$ the number density at radial position r, $\bar{\rho} = N/(4\pi R_{\mathrm{conf}}^3/3)$ the mean number density of the system, $\langle\cos^2\theta\rangle_r$ the mean value of $\cos^2\theta$ at radial position r, and s an empirical parameter varied between 0.5 and 0.7. Due to poor statistics for small values of r, the penalty function u_{pen} was only employed for $r \geq 3$ Å.

C. Correspondence between the dielectric and molecular models

We will now establish a link between the dielectric model described in Sec. II A and the simulated system described in Sec. II B. In both descriptions, R_{cav} denotes the radius at which the surrounding dielectric medium with dielectric constant $\varepsilon_{\mathrm{sur}}$ starts. Since the confining potential of the molecular model acts on the particle centers, the volume accessible to the particles is somewhat larger than that represented by the radius R_{conf}. To map the dielectric radius R_{diel}

TABLE I. Some parameters and properties of the simulated systems.

N	R_{conf} (Å)	R_{cav} (Å)	R_{diel} (Å)	δ (Å)	Δ (Å)
1200	19.74	20.4–60.0	20.6	0.9	−0.2–39.4
3000	26.79	27.4–60.0	27.6	0.8	−0.2–32.4
10 000	40.02	40.6–60.0	40.8	0.8	−0.2–19.2

of the dielectric model onto the molecular fluid of the simulated systems, we therefore expect the parameter δ defined by

$$\delta \equiv R_{diel} - R_{conf}, \tag{19}$$

to be larger than zero but smaller than the particle radius [see Fig. 1(b)]. Furthermore, δ is expected to be only weakly dependent on the curvature of the simulated system.

Simulated systems with the same R_{conf} (and the same N) but with different values of R_{cav} were fitted using a single value of R_{diel}. In the following, the simulated systems will be referred to through their values of N and Δ, where the latter is defined by

$$\Delta \equiv R_{cav} - R_{diel}. \tag{20}$$

Thus, Δ describes the strength of the coupling between the molecular fluid and the surrounding dielectric medium of the simulated systems, where $\Delta \to 0$ represents the full-coupling limit and $\Delta \to \infty$ the zero-coupling limit.

D. Simulation aspects

The properties of the model systems were determined by performing Monte Carlo (MC) simulations at constant number of particles, volume, and temperature. The particles were enclosed inside a spherical volume of radius R_{conf} with a hard-wall potential acting on the particle centers. The number of particles N in the system was $N=1200$, $N=3000$, and $N=10\,000$, and for each N a range of R_{cav} was used. Further details about the values used for the radii R_{conf} and R_{cav} are given in Table I. For most of the simulations, the dielectric constant ε_{sur} of the surroundings was set to 100. In addition to this, some simulations with $N=1200$ and $\Delta=0$ (see Sec. III C) were carried out using other values of ε_{sur}.

The MC simulations were performed using the standard Metropolis algorithm[14] with a translational displacement parameter of 0.5–0.7 Å and a rotational displacement parameter of 20°–25°. Each simulation involved 10^5-10^6 MC steps, each consisting of one trial move per particle. The integrated MC/molecular dynamics/Brownian dynamics simulation package MOLSIM (Ref. 15) for molecular systems was employed throughout. Statistical uncertainties were calculated using block averaging by subdividing each simulation into ten equally sized blocks.

E. Fluctuating multipole moment analyses

The contribution to the axial 2^ℓ-pole moment $Q_{\ell 0}$ from dipole i located at $\mathbf{r}_i=\{r_i, \theta_i, \varphi_i\}$ is given by

$$Q_{\ell 0,i} = \boldsymbol{\mu}_i \cdot \nabla[r_i^\ell P_\ell(\cos\,\theta_i)], \tag{21}$$

where $P_\ell(\cos\,\theta)$ represents the ℓ:th order Legendre polynomial. The moment $Q_{\ell 0}=\Sigma_i Q_{\ell 0,i}$ and its square $Q_{\ell 0}^2$ for $1\le\ell\le4$ of the molecular system was sampled 3 (for $N=1200$ and $N=3000$) and 1000 (for $N=10\,000$) times after each MC step using different orientations of the external Cartesian coordinate system.

The scaled simulated multipole moments $\hat{Q}_\ell(\Delta)$ were graphically fitted to the function given by Eqs. (5) and (6) with R_{diel} as the only fitting parameter. In principle, the dielectric constant ε_{diel} of the medium inside the cavity is also a fitting parameter; however, it turns out that the behavior of $\hat{Q}_\ell(\Delta)$ is relatively insensitive to ε_{diel}, given that ε_{sur} is large. Hence, we chose to use $\varepsilon_{diel}=100$ for all the fittings, leaving R_{diel} as the only parameter to be fitted.

In addition, the mean-square multipole moments $\langle Q_{\ell 0}^2\rangle$ were sampled for spherical subvolumes of varying radii, centered at the center of the simulated system. These analyses were made using systems with $\Delta=0$. Thereafter, the values of $\langle Q_{\ell 0}^2\rangle$ were used to calculate the dielectric constant ε using Eqs. (2) and (4). It should be noted that Eq. (2) is strictly only valid in the case when the dielectric constants ε_{diel} and ε_{sur} inside and outside of the dielectric sphere, respectively, are identical, which is not necessarily the case when sampling $\langle Q_{\ell m}^2\rangle$ near the confining surface. Nevertheless, it should give a reasonable approximation to the true value of ε_{diel}, and it is indeed not possible to determine the relationship between ε_{diel} and ε_{sur} *a priori* using the fluctuation approach used here.

IV. RESULTS AND DISCUSSION

A. Density profiles and orientational ordering

Figure 2(a) shows the relative density profile $\rho(r)/\bar{\rho}$, where $\bar{\rho}$ is the mean number density of the system, and the orientational distribution function $3\langle\cos^2\,\theta\rangle_r$. It is clear that the system without penalty functions (solid curves) is highly inhomogeneous and anisotropic; further analysis show that the particles are nearly close-packed at the cavity surface. In contrast, the density profile and orientation distribution obtained using the penalty function (dashed curves) maintain nearly constant values of unity, demonstrating that this ordering almost entirely vanishes. The disappearance of the anisotropic structure is confirmed by the results of Fig. 2(b), where the probability distribution $P(\cos\,\theta)$ for the outermost 2 Å of the molecular system is shown. The systematic deviation of $P(\cos\,\theta)$ from 1/2, which corresponds to an isotropic system, is at most $\approx$1%. The isotropic distributions were reached after 20 iterations of u_r and u_θ, each consisting of

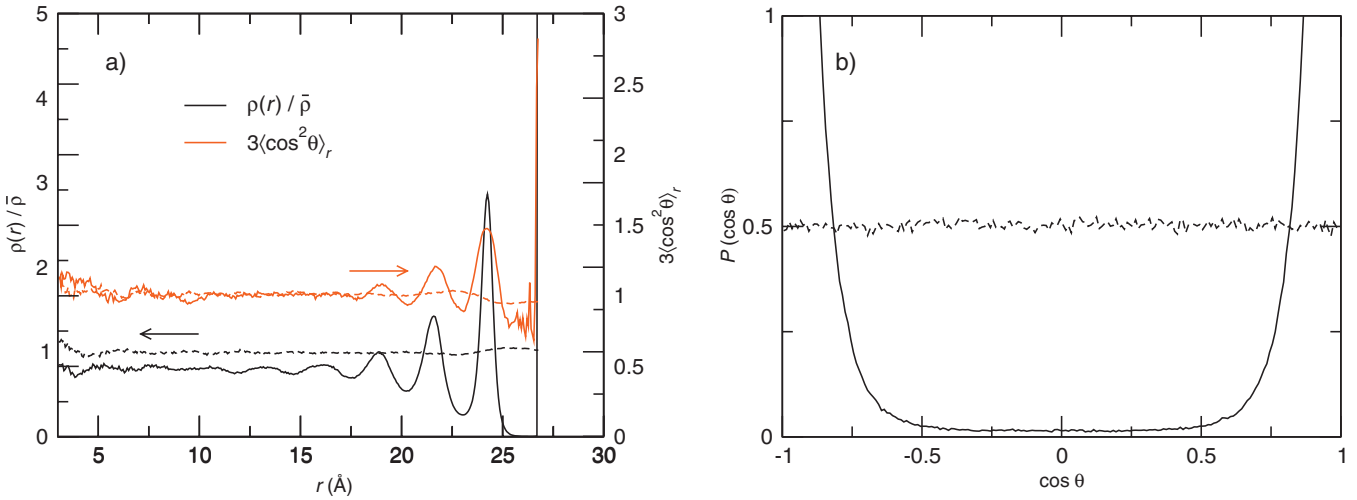

FIG. 2. (a) Relative density $\rho(r)/\bar{\rho}$ and orientation distribution $3\langle\cos^2\theta\rangle_r$ and (b) probability distribution of $\cos\theta$ for the outermost 2 Å of an IBC system of $N=3000$ particles with $\Delta=0$ without (solid curves) and with (dashed curves) converged penalty functions u_r and u_θ, according to Eqs. (17) and (18). The contact value of $\rho(r)/\bar{\rho}$ is ≈39.

1000 MC steps, in total corresponding to about 48 h of simulation time on a standard PC for the largest ($N=10\,000$) system. The simplicity and robust convergence behavior of the scheme leads us to the conclusion that the method prescribed here is a feasible one for creating a homogeneous and isotropic structure within the cavity.

In addition to the analysis of the structure of the system with respect to an external frame, the radial distribution function $g(r)$ and the probability distribution $P(\cos\theta_{dd})$ of the angle θ_{dd} formed by the dipole directions of two neighboring particles were analyzed. To enable a comparison between results from IBC and Ewald systems of equal density, an additional simulation using Ewald summation was carried at the density obtained by averaging the particle density inside a sphere of radius 35 Å centered at the origin of the IBC system with $N=10\,000$. For this Ewald simulation, $N=3000$ particles and box length $a=43.212$ Å were used; other parameters were identical to those given in Ref. 3. Figure 3(a) displays an excellent agreement between the two radial distribution functions, demonstrating a virtually identical radial structure of the two systems. Furthermore, Fig. 3(b) shows a very good agreement between the two angular distribution functions, even though a small discrepancy between the IBC and Ewald results is visible. This difference is reduced if the particles residing close to the surface in the IBC system are excluded from the analysis (data not shown), indicating that there is a remaining small effect of the surface on the dipole-dipole orientation. Nevertheless, these results show that the radial and angular distributions of the IBC and Ewald systems are essentially identical.

B. Electric fluctuations

In Fig. 4, we present the reduced multipole moment fluctuations $\hat{Q}_\ell(\Delta)$ as a function of the reduced parameter Δ/R_{diel}. The values of R_{diel} and δ obtained from the fits are

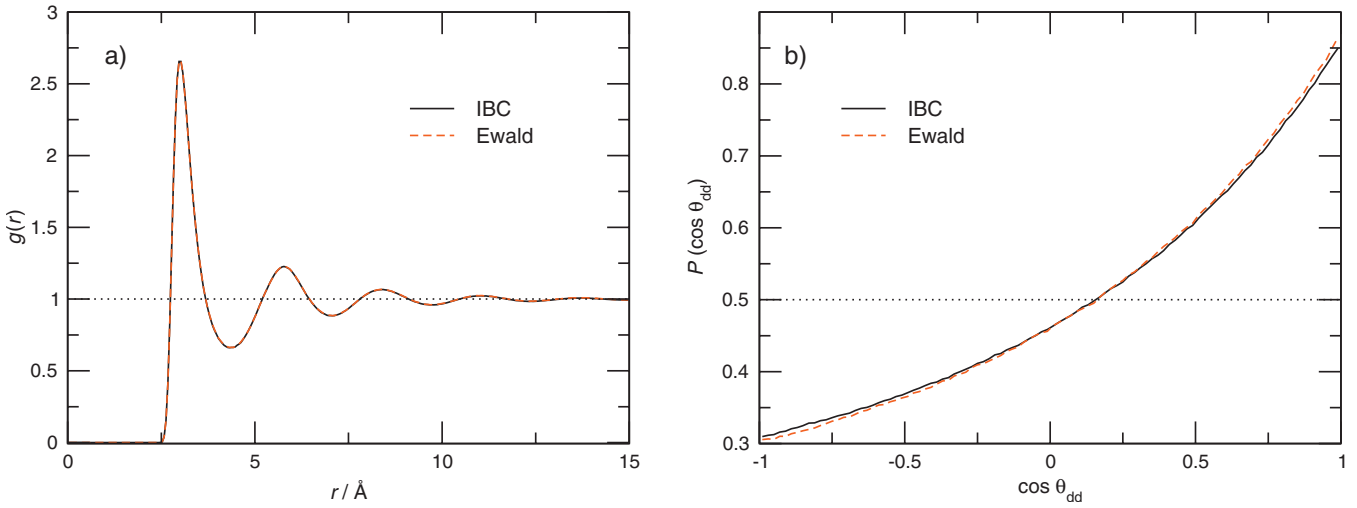

FIG. 3. (a) Radial distribution function $g(r)$ and (b) probability distribution $P(\cos\theta_{dd})$ of the dipole-dipole angle θ_{dd} of particles separated at most 4.2 Å for a system simulated using IBCs (solid curves) and Ewald summation (dashed curves). Homogeneous and isotropic distributions are also shown (dotted curves). For the IBC system, central particles located closer than r_{max} [15.0 Å for $g(r)$ and 4.2 Å for $P(\cos\theta_{dd})$] to the confining surface were excluded to avoid overlap between the sampling sphere and the surface. In (a), the two curves fully overlap each other.

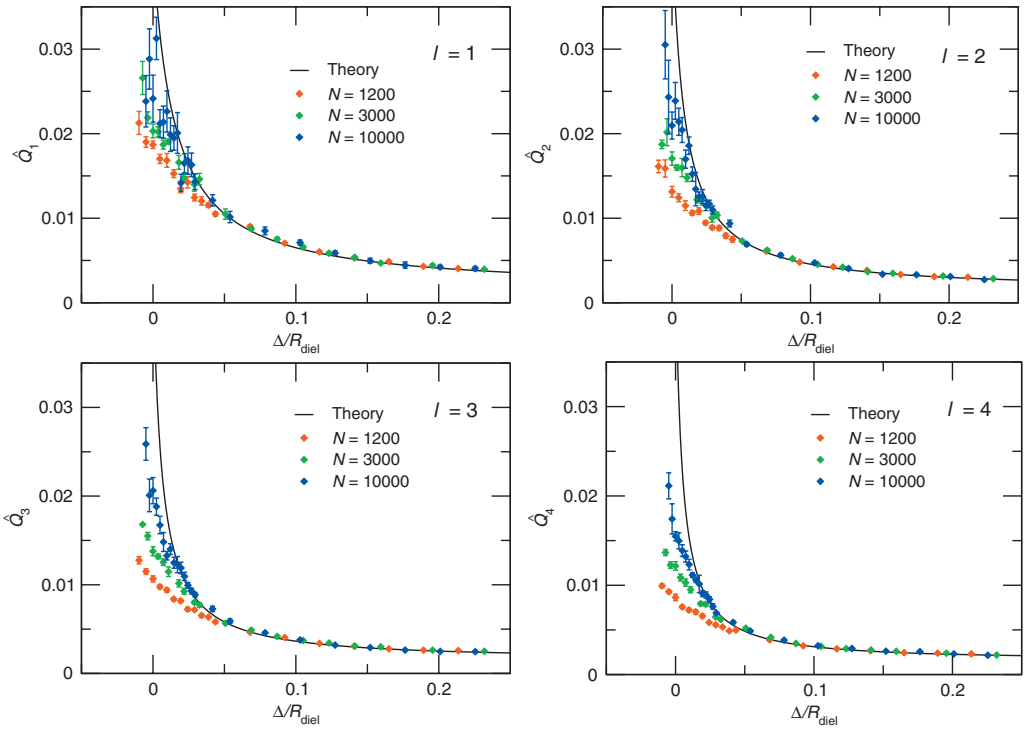

FIG. 4. Reduced multipole moment fluctuations $\hat{Q}_\ell(\Delta)$ as a function of the reduced parameter Δ/R_{diel} from theoretical predictions according to Eqs. (5) and (6) (solid curves) and simulation (symbols) at indicated ℓ. The error bars correspond to one standard deviation. The theoretical values at $\Delta=0$ are $\hat{Q}_1(0)=0.042$, $\hat{Q}_2(0)=0.045$, $\hat{Q}_3(0)=0.046$, and $\hat{Q}_4(0)=0.047$.

presented in Table I. For the smallest values of $R_{\text{cav}}-R_{\text{conf}}$, R_{diel} becomes larger than R_{cav}, thus making $\Delta<0$. This is of course theoretically ill-posed, but as long as $R_{\text{conf}}<R_{\text{cav}}$ it is nevertheless possible to simulate these systems. As assumed, the difference between the dielectric and confining radii, $\delta \approx 0.6(\sigma/2)$, is essentially N-independent, with only a weak effect arising from the curvature of the confining potential.

The dielectric model predicts increased multipole moment fluctuations as Δ/R_{diel} is reduced, with a pronounced maximum at $\Delta/R_{\text{diel}}=0$. Hence, as the coupling between the central region and the surrounding dielectric medium is enhanced, the probability of thermal fluctuations involving larger electrostatic moments increases. As can be seen from Fig. 4, the simulated values of $\hat{Q}_\ell(\Delta)$ are in quantitative agreement with those predicted by the dielectric model for $\Delta/R_{\text{diel}}>0.05$. However, at $\Delta/R_{\text{diel}}<0.05$ the simulated fluctuations for $1\leq\ell\leq4$ are (i) smaller than predicted by the dielectric model and (ii) N-dependent with a better agreement as N is increased. The latter observation indicates that the deviation from dielectric behavior may be due to the finite number of particles available to form the electric moments, which puts a limit on the magnitude of the fluctuations.

Even though the agreement between the dielectric and molecular models improves as the size of the simulated system is increased, the simulated values of $\hat{Q}_\ell(0)$ for $N=10\,000$ are still only half of those predicted by the dielectric model, given that the true value of $\varepsilon_{\text{diel}}$ is close to 100. This observation shows that the dielectric coupling is indeed very strong, in the sense that one needs to simulate systems with $N\gg10\,000$ to reach the dielectric limit.

C. Energetics

The total electrostatic energy per particle U_{el}/N of the simulated systems as a function of Δ for different system sizes is presented in Fig. 5. For values of Δ larger than about 1 Å, U_{el}/N is (i) independent of Δ and (ii) significantly different for systems of different size. Observation (i) implies that the coupling to the surrounding dielectric medium is negligible already at $\Delta\approx1$ Å, and observation (ii) can be attributed to the influence of the surface; in a smaller system, a larger fraction of the particles resides near the surface, where they experience a poorer solvation. Decreasing Δ to a sub-Ångström level leads to smaller U_{el}/N due to better sol-

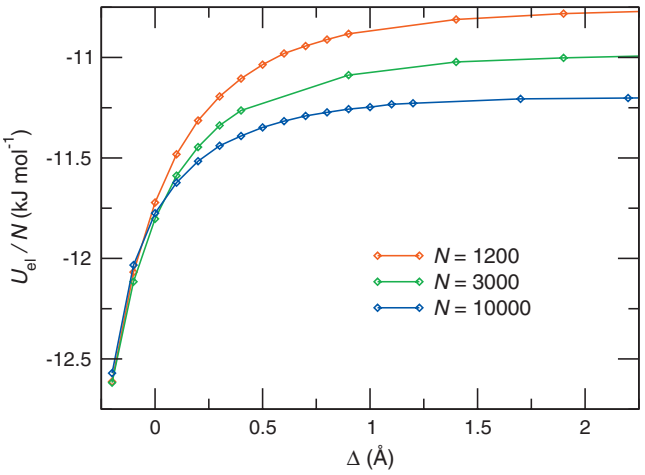

FIG. 5. Total electrostatic energy per particle U_{el}/N of the simulated systems as a function of Δ at indicated values of N.

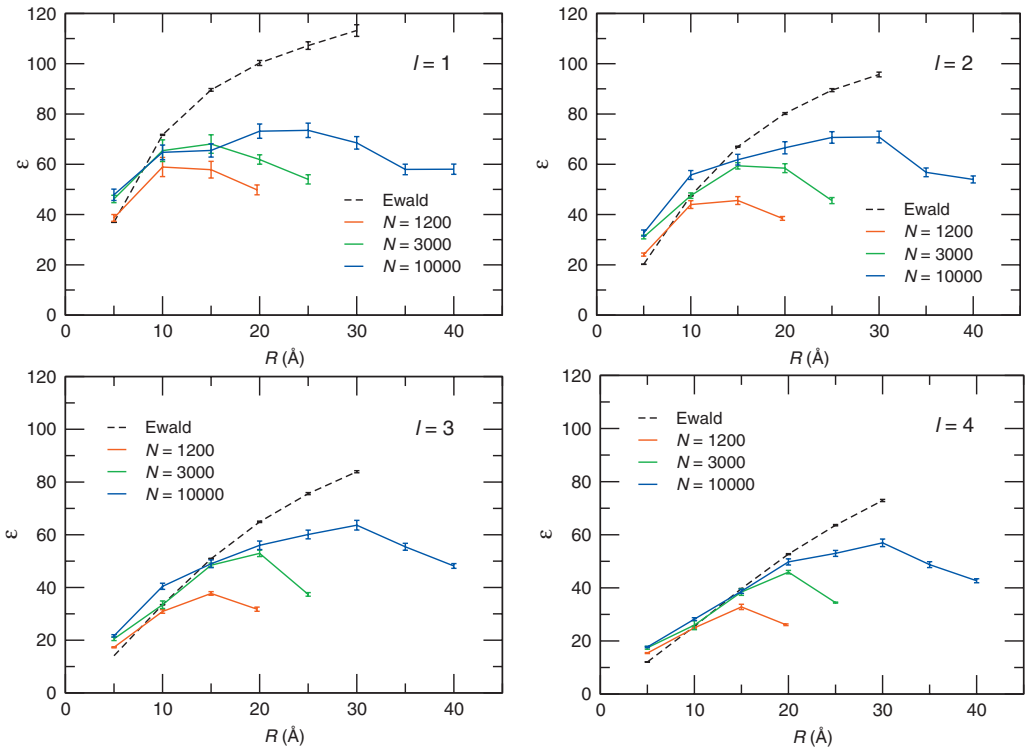

FIG. 6. Dielectric constant ε as a function of the radius R of the sampling sphere obtained from Eqs. (2) and (4) using electric moment fluctuations of order $1 \leq \ell \leq 4$ from simulated systems at indicated N and $\Delta = 0$. The error bars represent one standard deviation. Included also are results from simulations performed using the Ewald summation technique with $N = 100\,000$ (dashed curves).

vation of the particles near the surface, and as $\Delta \to 0$, U_{el}/N of the three systems essentially converge to the same value. The fact that the size dependence of U_{el}/N is strongly reduced as the system becomes more solvated is an indication that the system behaves energetically as a bulk system. This is also a further indication that the penalty functions previously described are successful in creating a bulklike structure of the system.

D. Dielectric constant

In Fig. 6, we present the dielectric constant ε of the molecular system calculated for spherical volumes of different radii using Eqs. (2) and (4). The dielectric constants were calculated at $\Delta = 0$ from the fluctuating electric moments with $1 \leq \ell \leq 4$ for different system sizes. Furthermore, we include the corresponding results obtained from a simulation using the Ewald summation technique with $N = 100\,000$. This system size allowed us to sample ε for sampling radii of up to 30 Å without any significant influence from the periodicity effects.[3] From the results obtained using IBCs we make the following observations:

(1) The dielectric constant initially increases as the radius R of the sampled sphere grows. However, as the boundary of the molecular system is approached, ε decreases. This boundary effect was previously observed by Wang and Hermans,[12] although it is much less pronounced in the present study, due to the stronger coupling to the surroundings used here.

(2) The dielectric behavior of the system is not converged at a length scale of 30 Å, in accordance with what we have previously observed from simulations using the Ewald summation technique.[3]

(3) As the order ℓ of the electric moment used for the calculation of ε is increased, the value of the dielectric constant at a given radius R becomes smaller. This is also in accordance with what we have observed before using the Ewald and RF techniques[3] and indicates that the dielectric behavior exhibits a slower convergence for moments of higher order.

(4) The IBC results start to diverge from the Ewald results around $R \approx R_{conf}/2$. If one assumes that the presented Ewald results are free from surface artifacts, this gives an indication of the range of the surface effects in the IBC scheme.

Observation 1 is indeed surprising, given that the dielectric medium outside the molecular system has a dielectric constant of 100, which is higher than any of the values calculated for the molecular system. This result further emphasizes the need for a very strong coupling to the surrounding medium by using a small value of Δ. One possible explanation for this observation is that the surrounding medium is approximated as a dielectric continuum, and as such only responds to the homogeneous part of the electrostatic field of the molecular system, neglecting polarization of higher order. Furthermore, observation 4 indicates that the range of the surface effects in the systems simulated using IBCs is similar to that found in Ewald simulations.[3] One point that needs to be stressed is the slight uncertainty in the density of

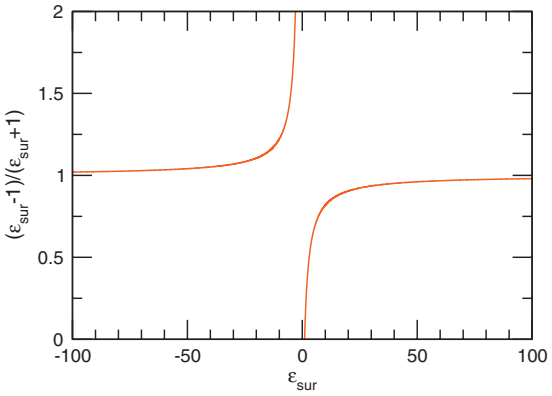

FIG. 7. The quota $(\varepsilon_{sur}-1)/(\varepsilon_{sur}+1)$ as a function of ε_{sur}. According to Eq. (9), this quota determines the strength of the coupling between the molecular system and the dielectric surroundings.

the IBC systems, compared with the well-defined density of the Ewald system, which could also have an effect on the dielectric constant.

E. The effect of varying ε_{sur}

Figure 7 shows the quota $(\varepsilon_{sur}-1)/(\varepsilon_{sur}+1)$ as a function of ε_{sur}. According to Eq. (9), in the image charge approximation this quota determines the strength of the electrostatic coupling between each particle in the molecular system and the dielectric surroundings. For a vacuum surrounding ($\varepsilon_{sur}=1$) the value of the quota is 0, whereas a value of 1 represents a conducting surrounding ($\varepsilon_{sur}=\pm\infty$). The quota then continues to increase toward infinity as ε_{sur} approaches -1 from below, corresponding to a continuously increasing coupling strength. In other words, a dielectric constant less than -1 implies that the resulting reaction field is *stronger* than the primary field that causes the response, but still pointing in a direction opposing the latter.

In Fig. 8, we present data of how the simulated dielectric constant ε of the molecular system depends on the dielectric constant ε_{sur} of the surrounding medium, starting from $\varepsilon_{sur}=100$. From these results, the following observations can be made:

(1) As the dielectric response of the surroundings is increased, the dielectric constant of the outer parts of the molecular system increases, thus reducing the boundary effects discussed above.
(2) The effect of varying ε_{sur} becomes smaller as the order ℓ of the multipole moment used for calculating ε is increased.
(3) At $\varepsilon_{sur}\approx -20$, the dielectric constant as calculated from the dipole moment fluctuations is greatly increased, indicating the appearance of a ferroelectric phase.

Observation 1 suggests that the use of a stronger dielectric response of the surroundings than that expected from the molecular system, even resorting to negative values of ε_{sur}, can be a way to reduce the surface effects present in the IBC method. The use of a negative dielectric constant for the surroundings may seem unphysical, since this is clearly not representative of the macroscopic value of ε for the molecular system being simulated. However, it was shown in a recent study[16] that the *local* dielectric response in a strongly polar liquid indeed corresponds to a negative value of ε.

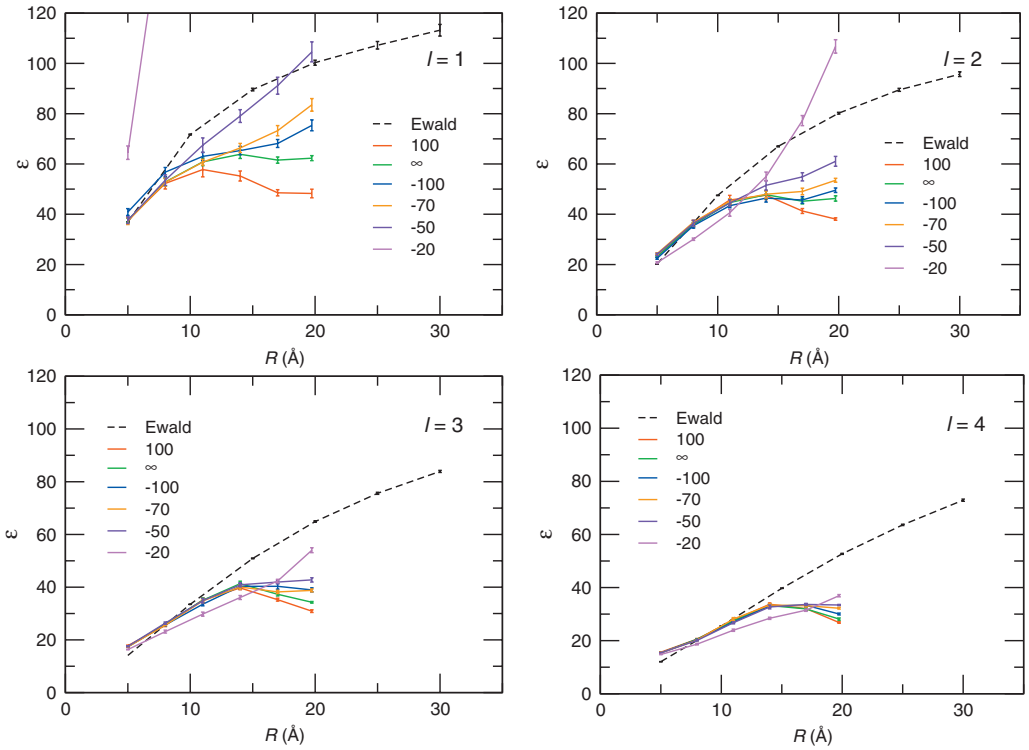

FIG. 8. Dielectric constant ε as a function of the radius R of the sampling sphere obtained from Eqs. (2) and (4) using electric moment fluctuations of order $1\leq\ell\leq 4$ from simulated systems with $N=1200$ and $\Delta=0$ at indicated ε_{sur}. The error bars represent one standard deviation. Included also are results from simulations performed using the Ewald summation technique with $N=100\,000$ (dashed curves).

Since the solvation of the outermost layer of molecules occurs on a length scale of a few angstroms, it should indeed be more appropriate to use the local rather than the expected macroscopic value of ε_{sur}. As for observation 2, we attribute this to the fact that the solvation of the higher order moments becomes increasingly more short-range in its character. A consequence of this is that it becomes harder to accomplish a bulklike representation of the boundary between the molecular system and the dielectric continuum as ℓ is increased, which is reflected in the fact that the higher order moments become increasingly more difficult to solvate. The problems in removing the surface effects for the higher order moments once again stresses the difficulties present in trying to fully solvate a molecular system using a dielectric continuum surrounding.

Assuming that the results from the Ewald simulation well represent a "true" bulk system, the most realistic results employing IBC's are obtained using a surrounding dielectric medium with $\varepsilon_{sur}=-50$. It should be noted, however, that a considerable system size dependence was observed when making the corresponding analysis (data not shown) for systems with larger N. In particular, the ferroelectric phase appeared at more negative values of ε_{sur}, corresponding to a weaker coupling with the surroundings (see Fig. 7), as N was increased. One may therefore regard ε_{sur} as an empirical parameter that should be adjusted for the particular system under study in order to minimize the surface effects.

V. CONCLUSIONS

The present study shows that it is indeed possible to simulate a bulklike system using IBCs and obtain radial and angular distributions virtually identical to those obtained from applying the Ewald summation. To reduce the effects of the hard wall confining the molecular system, we have found that (i) the response from the surrounding dielectric medium has to be applied very close to the boundary of the molecular system and (ii) properly adjusted penalty functions are effective in suppressing inhomogeneous and anisotropic distributions of particles near the hard wall. Furthermore, we have found that using a dielectric continuum with the same dielectric constant as that of the molecular system to describe the surroundings does not provide a sufficiently strong solvation of the simulated system. This solvation deficiency could partly be remedied by using a stronger coupling between the molecular system and the surroundings, manifested in a negative dielectric constant of the surrounding dielectric medium.

For the systems investigated ($N \leq 10\,000$), the extension of the region free from boundary artifacts scales approximately linearly with the length-scale of the system. However, (i) the increasingly improved correspondence between the dielectric model and the simulated data at increasing N (Fig. 4) and (ii) the fact that our model system approaches a true macroscopic system in the thermodynamic limit, with or without a dielectric correction at the boundary, implies that the extension of the region affected by the boundary should become negligible as $N \to \infty$. In the case of the Ewald summation technique, the effects of the imposed periodicity of the infinite system extends into volumes of radius $R \approx L/4$, with L being the side length of the primary box.[3] Thus, the region affected by the boundary conditions scales linearly with the length scale of the simulated system also in this case. However, for the Ewald summation technique there are no arguments that this length-scale dependence should be weakened as $N \to \infty$ and no such weakening was observed for $N \leq 300\,000$.[3]

The observed slow convergence behavior of ε with the radius R of the sampling sphere emphasizes the need of simulating very large systems to reach bulk dielectric behavior, and from the present results it is indeed not possible to draw any conclusions about when this behavior will be reached. Since this was observed also for systems simulated using the Ewald and RF methods, and hence seems to be a method-independent effect, we argue that this slow convergence is a true physical property of strongly polar systems.

It should be noted that simulating more realistic molecular liquids such as water using the IBC approach is not as straightforward as simulating a simple Stockmayer fluid. In particular, the design of penalty functions would need to be taken extra care of, and maintaining the proper hydrogen-bonding structure would probably not be possible close to the confining surface. Furthermore, we have not assessed the dynamics of the IBC system as compared with, for example, a system simulated using the Ewald summation technique.

Regarding the computational performance of the various methods described above, it should be mentioned that systems simulated using IBCs exhibit an $\mathcal{O}(N^2)$ scaling behavior, whereas the classic implementation of the Ewald method scales as $\mathcal{O}(N^{3/2})$, thus making the latter method more appealing from a computational point of view. However, in the same way as the Ewald method has been optimized to yield an $\mathcal{O}(N \log N)$ behavior using the so-called particle-particle particle-mesh Ewald method,[17] it is possible to optimize the IBC scheme to facilitate the simulation of significantly larger systems.

In conclusion, we have demonstrated here that systems simulating using IBCs in practice suffer from boundary effects of range and magnitude similar to what was previously found for the Ewald and RF techniques, even though the effects originate from very different sources. Whether the IBC or Ewald/RF technique is best suited for simulating dielectric properties of molecular systems thus remains an open question.

ACKNOWLEDGMENTS

Financial support by the Swedish Research Council (VR) through the Linnaeus grant for the Organizing Molecular Matter (OMM) center of excellence and computer time at LUNARC are gratefully acknowledged. Furthermore, we would like to thank Håkan Wennerström for helpful scientific discussions.

[1] P. Ewald, Ann. Phys. **369**, 253 (1921).
[2] J. A. Barker and R. O. Watts, Mol. Phys. **26**, 789 (1973).
[3] J. Stenhammar, G. Karlström, and P. Linse, J. Chem. Phys. **131**, 164507 (2009).
[4] P. H. Hünenberger and J. A. McCammon, Biophys. Chem. **78**, 69 (1999).
[5] M. A. Kastenholz and P. H. Hünenberger, J. Phys. Chem. B **108**, 774

(2004).
[6] F. Figueirido, G. S. Del Buono, and L. M. Levy, J. Chem. Phys. **103**, 6133 (1995).
[7] X. Wu and B. R. Brooks, J. Chem. Phys. **122**, 044107 (2005).
[8] M. A. Kastenholz and P. H. Hünenberger, J. Chem. Phys. **124**, 124108 (2006).
[9] H. L. Friedman, Mol. Phys. **29**, 1533 (1975).
[10] J. D. Jackson, *Classical Electrodynamics*, 3rd ed. (Wiley, New York, 1999).
[11] A. Wallqvist, Mol. Simul. **10**, 13 (1993).
[12] L. Wang and J. Hermans, J. Phys. Chem. **99**, 12001 (1995).
[13] J. Stenhammar, P. Linse, P.-Å. Malmqvist, and G. Karlström, J. Chem. Phys. **130**, 124521 (2009).
[14] N. Metropolis, A. W. Rosenbluth, M. N. Rosenbluth, A. H. Teller, and E. Teller, J. Chem. Phys. **21**, 1087 (1953).
[15] P. Linse, *MOLSIM* (Lund University, Sweden, 2009).
[16] G. Karlström, P. Linse, and C. E. Woodward, J. Chem. Phys. **132**, 084508 (2010).
[17] A. W. Appel, SIAM (Soc. Ind. Appl. Math.) J. Sci. Stat. Comput. **6**, 85 (1985).